

Ab Initio Study of Magnesium and Magnesium Hydride Nanoclusters and Nanocrystals: Examining Optimal Structures and Compositions for Efficient Hydrogen Storage

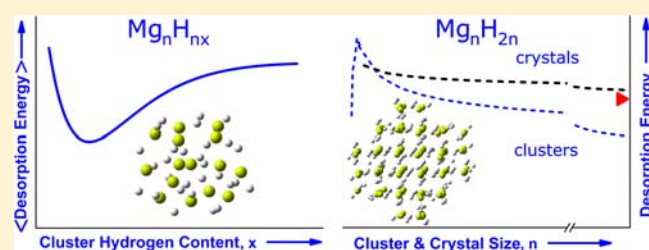
Emmanuel N. Koukaras,^{*,†,‡} Aristides D. Zdetsis,^{*,†} and Michael M. Sigalas[§]

[†]Molecular Engineering Laboratory, Department of Physics and [§]Department of Material Science, University of Patras, Patras 26500 GR, Greece

[‡]Institute of Chemical Engineering Sciences, Foundation for Research and Technology-Hellas (FORTH/ICE-HT), GR-26504 Patras, Greece

S Supporting Information

ABSTRACT: On the basis of the attractive possibility of efficient hydrogen storage in light metal hydrides, we have examined a large variety of Mg_nH_m nanoclusters and $(MgH_2)_n$ nanocrystals ($n = 2-216$, $m = 2-436$) using high level coupled cluster, CCSD(T), *ab initio* methods, and judiciously chosen density functional calculations of comparable quality and (near chemical) accuracy. Our calculated desorption energies as a function of size and percentage of hydrogen have pinpointed optimal regions of sizes and concentrations of hydrogen which are in full agreement with recent experimental findings. Furthermore, our results reproduce the experimental desorption energy of 75.5 kJ/mol for the infinite system with remarkable accuracy (76.5 ± 1.5 kJ/mol).



1. INTRODUCTION

Hydrogen may be the fuel of the future replacing hydrocarbons because of its higher performance (in fuel cells), much higher gravimetric energy density, and negligible environmental implications, in comparison to hydrocarbons. However, the main problem, and consequently the focus of current-day research, is the efficient storage of significant amounts of hydrogen with the smallest possible weight. One (among many) possible solution is the storage of hydrogen in metal hydrides because of the moderate temperature and pressure conditions required. In particular Mg hydride is one of the most prominent materials with reversible hydrogen capacity of up to 7.6% wt.^{1,2}

More recently, nanostructure metal hydrides³⁻⁶ have been also proposed for hydrogen storage due to their expected higher diffusivity and their higher surface to volume ratios. These characteristics are expected to lead to improved reaction kinetics, reduced enthalpy of formation, and lower hydrogen absorption and release temperatures⁴ due to the different destabilization energies of the metal clusters and their corresponding hydrides.^{5,6} Thus, reduction of the MgH_2 particle size to the nanoscale has been suggested, by both theoretical⁵ and experimental⁷⁻¹² evidence, as a possible means for tuning up the desorption thermodynamics.⁶

Previous theoretical studies of various levels of complexity, from Hartree-Fock (HF) and density functional theory (DFT)⁵ to Quantum Monte Carlo (QMC),⁶ have mainly focused on MgH_2 (or Mg_nH_{2n}) nanoparticles, in which at some limited cases ($n = 6, 9$, and 15) stepwise desorption has been

considered by successively removing H_2 molecules.⁵ In the present investigation, using high level CCSD(T) *ab initio* (for the smaller clusters) and improved DFT methods of comparable quality and (high) accuracy, we have considered the reverse process of hydrogen sorption on bare Mg_n clusters. We have examined hydrogenated Mg_nH_m clusters of small and medium sizes, in which hydrogen atom pairs (H_2 , $H+H$) were gradually added, starting from a large variety of low energy bare Mg_n clusters. At each level of hydrogenation the Mg_nH_m clusters were generated from several energetically lower Mg_nH_{m-2} structures by the addition of a $H+H$ pair each time. This way, we can safely and rather accurately study in a stepwise and stoichiometry-unbiased way, not only the size dependence of (de)sorption energy, but also its variation with hydrogen content, structure, and composition. This plan, which allows the location and identification of optimal regions of both n (size) and m (composition), has been carried out very successfully for a large variety of small and medium Mg_nH_m nanoclusters of sizes up to a few nanometers. At the same time, we have constructed large stoichiometric $(MgH_2)_N$ nanocrystals of various sizes ($N = 48, 120, 169, 216$) based on the bulk MgH_2 structure in order to study the size dependence all the way up to the infinite MgH_2 crystal. For these particular nanocrystals, which are all of the same morphology, the desorption energy $\Delta E_d(MgH_2)_N$ would be expected, on the basis of general arguments based on the relative number of bulk

Received: June 29, 2012

Published: August 24, 2012

Table 1. Binding energies (D_e) in eV of Mg_4 , Mg_6H_{12} and Mg_4H_8 , Mg_6H_{12} Clusters, Calculated with a Variety of Functionals, and CCSD(T) Single-Point Calculations at the Corresponding DFT, and CCSD (Last Column) Optimized Geometries

structure	property	PBE	BP86	PW91	B97D	TPSSh	B3LYP	M05-2X	M05	M06-2X	M06	CCSD(T)
Mg_4	De/cc-pVTZ (eV)	1.55	1.21	1.55	1.22	1.51	0.57	0.87	1.42	0.98	1.38	
	De/CCSD(T) (eV)	1.02	1.02	1.02	1.00	1.01	1.01	1.00	1.02	1.02	1.00	1.01
Mg_4H_8	De/cc-pVTZ (eV)	21.93	22.84	22.22	23.30	24.29	22.43	19.52	22.84	22.25	23.21	
	De/CCSD(T) (eV)	22.82	22.82	22.82	22.81	22.82	22.81	22.81	22.80	22.80	22.82	22.82
Mg_6	De/cc-pVTZ (eV)	2.49	1.90	2.49	1.88	2.37	0.82	1.47	2.30	1.63	2.22	
	De/CCSD(T) (eV)	1.62	1.62	1.62	1.56	1.62	1.58	1.59	1.62	1.62	1.60	1.58
Mg_6H_{12}	De/cc-pVTZ (eV)	34.23	35.56	34.69	36.31	37.86	35.00	34.29	35.64	34.94	36.42	
	De/CCSD(T) (eV)	35.75	35.75	35.75	35.74	35.75	35.75	35.75	35.72	35.72	35.75	35.76

versus surface atoms,^{13–16} to obey the size dependence of the form:

$$\Delta E_d((MgH_2)_N) = a + b \cdot N^{-1/3}$$

As will be illustrated in what follows, this relation is indeed obeyed remarkably accurately. Not only that, but the value for the parameter a obtained here, which is the predicted value of $\Delta E_d(MgH_2)_N$ for the infinite crystal ($N \rightarrow \infty$), is 76.5 ± 1.5 kJ/mol. This value is unexpectedly (and rather unbelievably) close to the experimental value of 75.5 kJ/mol for the infinite MgH_2 solid. This type of agreement is highly suggestive about the validity of the present approach and the quality and accuracy of our results (for the desorption energy as a function of both n and m in addition to N) which are presented in sections 3 and 4, after a short description of the theoretical techniques in section 2.

2. THEORETICAL AND COMPUTATIONAL TECHNIQUES

The initial geometries of the lowest and lower energy bare Mg_n clusters have been obtained from the literature.^{17–19} For several smaller Mg_n clusters ($n = 2–7$), these geometries have been further optimized, compared, and reevaluated using *ab initio* many-body Møller–Plesset perturbation theory of second order (MP2), and coupled-cluster theory, including singlet and doublet excitations (CCSD). At the equilibrium geometries, single-point energy calculations were performed using higher level methods, such as CCSD(T), which includes triplet excitations noniteratively.^{20,21} These calculations have been performed with the correlation consistent cc-pVTZ basis set²² of triple- ζ quality, using the Gaussian program package.²³ The fully *ab initio* results for representative small clusters (such as Mg_4 and Mg_6) have been compared with similar optimization (and single point) calculations using density functional theory (DFT). For the DFT calculations we have employed a variety of popular as well as recently developed functionals, within the generalized-gradient approximation (GGA), hybrid GGA, and hybrid meta-GGA functionals, such as PBE,²⁴ BP86,^{25,26} PW91,²⁷ B97D,²⁸ B3LYP,^{29,30} TPSSh,^{31,32} M05,³³ and M06,³⁴ in order to assess the suitability of, and decide the “proper”, functional(s) for, the present investigation. For this purpose, the full plan (*ab initio* CCSD(T) and DFT with a large variety of classical and modern functionals) was followed for the hydrogenated Mg_nH_m nanoclusters, using primarily (but not solely) as benchmark systems the corresponding Mg_4H_8 and Mg_6H_{12} clusters, which were generated using the procedure which will be described below. For these DFT calculations we

have employed the TURBOMOLE³⁵ and GAMESS³⁶ packages using the same basis set (cc-pVTZ). For the purpose of the present calculations the main property of interest is the desorption energy, which is based on energy differences between hydrogenated and non-hydrogenated systems and not absolute binding energies. The total or non-normalized desorption, $\Delta E_{\text{dtot}}(Mg_nH_{2n})$, for a Mg_nH_{2n} nanocluster or nanocrystal is defined as usual by the relation

$$\Delta E_{\text{dtot}}(Mg_nH_{2n}) = nE(H_2) + [E(Mg_n) - E(Mg_nH_{2n})] \quad (1)$$

whereas the normalized per H_2 mole desorption energy, $\Delta E_d(Mg_nH_{2n})$, is given as

$$\Delta E_d(Mg_nH_{2n}) = E(H_2) + [E(Mg_n) - E(Mg_nH_{2n})]/n \quad (2)$$

In both relations, besides the total energy of the H_2 molecule, $E(H_2)$, the desorption energy is fully determined by the energy difference of the Mg_n and Mg_nH_{2n} clusters, $E(Mg_n)$ and $E(Mg_nH_{2n})$ respectively. It is important to emphasize that in all the above total energies we include zero-point energy (ZPE) corrections; that is, $E(H_2) = E_0(H_2) + ZPE(H_2)$, $E(Mg_n) = E_0(Mg_n) + ZPE(Mg_n)$, and $E(Mg_nH_{2n}) = E_0(Mg_nH_{2n}) + ZPE(Mg_nH_{2n})$, where E_0 , in an obvious notation, is the total electronic energy without ZPE.

It is clear, therefore, that the “ideal” or “desirable” DFT method has to perform equally well, or at least just about equally well, for both Mg_n and Mg_nH_{2n} . Representative benchmarking comparisons for the binding energies of both types of “stoichiometric” clusters with $n = 4$ and 6 respectively are summarized in Table 1. For each of the functionals in Table 1 we have performed geometry optimizations in order to calculate and provide the binding energy as given by the specific functional (at the optimized geometry using this particular functional). Additionally we provide the binding energy as calculated by single point CCSD(T) at the geometry produced by the corresponding functional, in comparison to the geometry produced by optimization using the coupled clusters (CCSD) method (last column). These values act as a criterion on the quality of both energy and geometry. Most interestingly, as we can see from Table 1, the GGA functionals PBE, BP86, and PW91 lead to the best geometries but, as would be expected, not to the best (or even acceptable in some cases) binding energies. The performance of the dispersion corrected GGA functional B97D differs between hydrogenated (better) and non-hydrogenated (worst) systems. Surprisingly, the hybrid functionals TPSSh and B3LYP overestimate and underestimate the binding energies, respectively.

The most promising methods among those studied here belong to the $M0n$ family, although even in this case the performance varies. The $M0n-2X$ functionals produce the most accurate binding energies for the pure systems, while M05 produces exceptional binding energies for the hydrogenated systems. However, for calculating binding energy differences (desorption energies) the method to be chosen is required to perform in a similar and consistent manner for both systems (pure and hydrogenated). In this respect, the M06 functional is the best choice, fulfilling these requirements. M06 produces high quality geometries, although it overestimates the binding energy, but in a systematic manner, which allows the calculation of accurate desorption energies. These conclusions are not affected when the basis set superposition error (BSSE) is accounted for in the calculations. The BSSE correction, calculated using the counterpoise correction method (CP), is very small (although not marginal) and does not influence the average relative performance of the functionals in Table 1 (see Table S1 in the accompanying Supporting Information).

The advantages of the M06 functional for such calculations, emerging from Table 1, have been also confirmed by additional selective calculations (limiting the range of functionals studied) for representative larger and nonstoichiometric nanoclusters such as Mg_8H_8 and $Mg_{11}H_{10}$. These results are shown in Table 2.

Table 2. Binding energies (D_e) in eV of Mg_8 , Mg_8H_8 and Mg_{11} , $Mg_{11}H_{10}$ Clusters, Calculated with the M06 (for $n = 8$ and $n = 11$), and PBE, BP86, and B3LYP (for $n = 8$) Functionals, Together with CCSD(T) Single-Point Calculations at the Corresponding DFT Optimized Geometries

structure	property	PBE	BP86	B3LYP	M06
Mg_8	De/cc-pVTZ (eV)	4.09	3.16	1.41	3.77
	De/CCSD(T) (eV)	2.97	2.96	2.90	2.94
Mg_8H_8	De/cc-pVTZ (eV)	24.39	24.68	23.14	25.49
	De/CCSD(T) (eV)	24.55	24.56	24.57	24.56
Mg_{11}	De/cc-pVTZ (eV)				6.71
	De/CCSD(T) (eV)				5.72
$Mg_{11}H_{10}$	De/cc-pVTZ (eV)				33.63
	De/CCSD(T) (eV)				32.11

Therefore, the majority of the present computations (geometries and energies) have been performed with the

M06 functional. In addition, for the very large size clusters and nanocrystals, since PBE with significantly lower computational cost produces very good geometries (as can be seen from Table 1), the DFT geometry optimizations have been performed with the PBE functional, using the resolution of the identity approximation.³⁷ The energies are, then, evaluated by single point M06 calculations at these (PBE) geometries, with substantial computational savings, without sacrificing accuracy. This is very important for the very large number and variety of initial structures considered here for each composition.

The construction of the initial structures of the Mg_nH_m clusters follows a long, complicated, systematic and reliable "algorithm": For a given number, n , of Mg atoms we establish a large (wherever possible) number of lowest, lower, and low-lying bare Mg_n isomers (the number of isomers increases with n). For a given isomer we then start the process of stepwise hydrogenation by adding two H atoms at a time. A nearly exhaustive search is performed, using symmetry unrestricted geometry optimizations (C_1) at the DFT/PBE and/or DFT/M06 level(s) to determine, among a very large (especially for larger n) set of possible positions, the energetically best (second best, third best, etc.) hydrogenated sites. Having established several low-lying Mg_nH_2 structures the second pair of hydrogen atoms (for the same number of Mg atoms, n) was again tested in a similar way, by full unrestricted reoptimization (including reconstruction), to establish the best low-lying structures of Mg_nH_4 clusters. This process was repeated again (for a given n) up to Mg_nH_{2n+4} , and in some cases up to Mg_nH_{2n+6} , well above the Mg_nH_{2n} stoichiometry. We have also considered Mg_nH_m geometry optimizations starting from the geometries of the $Mg_{n-1}H_m$ cluster with the addition of one Mg atom. Thus, the whole cycle of optimizations includes, for a given n , a significant portion of all conceivable possible energetically low lying isomers in each intermediate and final level of hydrogenation. In Figure 1, we show representative lowest energy structures for small/medium Mg_nH_m nanoclusters obtained by the process outlined above.

The same process for the larger Mg_nH_m nanoclusters has produced the representative results of Figure 2. For the lowest energy structures in each case, vibrational analysis has been performed to determine the zero-point energy (ZPE) correction and to test the dynamical stability (no imaginary frequency modes) of the particular cluster.

In addition to the Mg_nH_m and Mg_nH_{2n} nanoclusters obtained and optimized as described, we have also constructed and

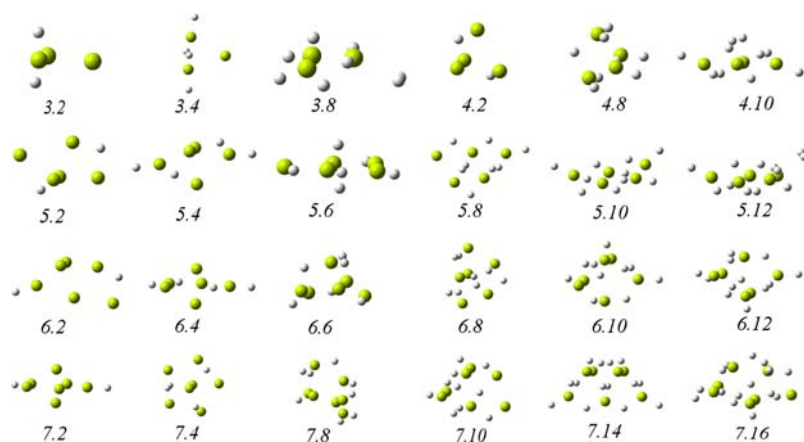


Figure 1. Lowest energy geometries obtained here at the DFT/M06 level of theory for representative Mg_nH_m , $n = 3-7$, $m = 2-16$ clusters.

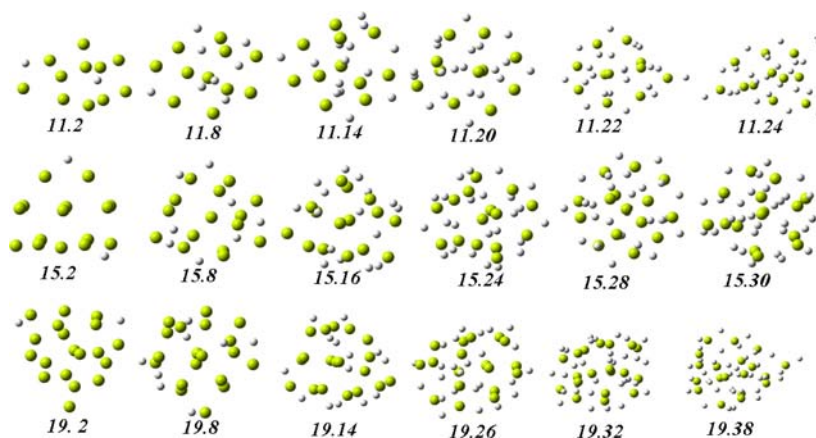


Figure 2. Representative lowest energy structures for the larger Mg_nH_m ($n = 11-19$, $m = 2-38$) clusters.

optimized at the same level(s) of theory large stoichiometric nanocrystals $(\text{MgH}_2)_N$ (with $N = 48, 120, 169$, and 216) of fixed composition and symmetry based on the bulk MgH_2 structure. The properties of these nanocrystals are expected to approach the bulk properties as N increases, approaching infinity. Thus, for accurate finite size results, extrapolation to infinity would be expected to reproduce the results of the infinite MgH_2 solid at a similar accuracy. As will be shown this is indeed the case. The results for the desorption energy of the MgH_2 solid obtained here are unexpectedly close (within chemical accuracy) to the experimental value. Therefore, the results presented here are expected to be of similar chemical accuracy.

3. RESULTS AND DISCUSSION FOR Mg_nH_m NANOCCLUSERS

3.1. Size-Dependence of Desorption Energy of Mg_nH_{2n} Nanoclusters. The size-dependence of the desorption energy, in particular for small and medium size Mg_nH_{2n} nanoclusters, is of primary importance. This is due to the expectations of achieving lower desorption energies and temperatures as the crystalline size is reduced. Such expectations have motivated analogous (but not similar) work in the past.⁵ The desorption energy of the Mg_nH_{2n} clusters with $n = 3-19$ obtained in this work following the full procedure (using a nearly exhaustive optimal geometry search) outlined in section 2 is plotted in Figure 3 as a function of the size, n , of the cluster. In the same figure, we have plotted for comparison the results of Wu et al.⁶ obtained by the fixed-node diffusion Monte Carlo (DMC) method. As we can see, both results are of comparable quality. In the same figure we have also included some “isolated” results for $n = 25$ and $n = 32$, obtained with a limited number of initial geometries based in some partially optimized bulk fragments. It is interesting to observe that these values are also in close agreement to the DMC results. This point will be discussed further in section 4. As it is clear from Figure 3, desorption energies lower than the bulk values (around 75 kJ/mol) are obtained only for $n < 6$, which is extremely small (maximum diameter of about 0.5 nm).

Instead $\Delta E_d(\text{Mg}_n\text{H}_{2n})$ achieves a maximum value of about 95 kJ/mol, around $n = 11$, and then it starts decreasing monotonically, as shown in Figure 3. This decrease in $\Delta E_d(\text{Mg}_n\text{H}_{2n})$ for larger sizes, which is common to both nanoclusters and nanocrystals, is expected to continue monotonically to the very large n values (theoretically all the

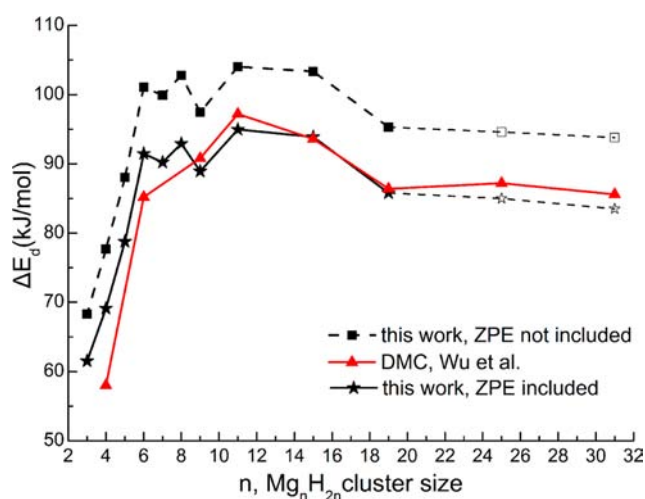


Figure 3. Desorption energy $\Delta E_d(\text{Mg}_n\text{H}_{2n})$, in kJ/mol, as a function of n , obtained here (solid stars and squares) at the DFT/M06 level of theory, with ZPE (solid stars) and without ZPE (solid squares) corrections, in comparison to the results of the DMC method (triangles). The empty stars and squares denote results obtained with a limited number of sampling for alternative geometries.

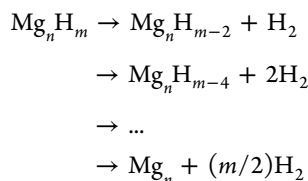
way to $n \rightarrow \infty$), not necessarily with the same n -dependence ($\sim n^{-1/3}$) as for the bulk-like nanocrystals, and not necessarily to the same asymptotic bulk value (of about 75.5 kJ/mol). We will examine this behavior in section 4 in parallel with the nanocrystal structures. It is clear, however, from the results obtained so far in Figure 3, that size reduction of the nanocrystals by itself (except for the unrealistic case of $n < 6$) cannot significantly improve the desorption energy (and temperature) value of bulk MgH_2 , unless, perhaps, other factors such as variation of stoichiometry could be helpful. This is examined in the next section.

3.2. Hydrogen Percentage Dependence of Desorption Energy for Mg_nH_m Nanoclusters. For the nonstoichiometric Mg_nH_m clusters, the above definitions eqs 1 and 2 for desorption energy should be obviously modified as

$$\Delta E_{\text{d,tot}}(\text{Mg}_n\text{H}_m) = (m/2)E(\text{H}_2) + [E(\text{Mg}_n) - E(\text{Mg}_n\text{H}_m)] \quad (3)$$

$$\Delta E_d(\text{Mg}_n\text{H}_m) = E(\text{H}_2) + 2[E(\text{Mg}_n) - E(\text{Mg}_n\text{H}_m)]/m \quad (4)$$

For such clusters, besides the “absolute” desorption energy $\Delta E_d(\text{Mg}_n\text{H}_m)$ defined above, we can consider the “stepwise desorption energy” ΔE_{sd} for the stepwise process:



in which a hydrogen molecule is removed (or added in the reverse process) one at a time. In this case, the relative or stepwise desorption energy ΔE_{sd} can be defined in relation to the energy of the $\text{Mg}_n\text{H}_{m-2}$ structure of the previous step, rather than with respect to the bare magnesium cluster, as follows:

$$\Delta E_{sd}(\text{Mg}_n\text{H}_m) = E(\text{H}_2) + [E(\text{Mg}_n\text{H}_{m-2}) - E(\text{Mg}_n\text{H}_m)] \quad (5)$$

Furthermore, since at each stage the (de)sorption energy can be defined with respect to the $m - 2$ or with respect to the $m + 2$ structure (stage), it is more appropriate to define a smoother stepwise desorption, ΔE_{ssd} , as an average of the two alternatives. Thus, the “average” desorption energy is given as

$$\begin{aligned} \Delta E_{ssd}(\text{Mg}_n\text{H}_m) &= E(\text{H}_2) + [(E(\text{Mg}_n\text{H}_{m-2}) - E(\text{Mg}_n\text{H}_m)) \\ &\quad + (E(\text{Mg}_n\text{H}_m) - E(\text{Mg}_n\text{H}_{m+2}))]/2 \end{aligned}$$

or for the more general k -step case:

$$\begin{aligned} \Delta E_{ssd}(\text{Mg}_n\text{H}_m) &= E(\text{H}_2) + [E(\text{Mg}_n\text{H}_{m-2k}) \\ &\quad - E(\text{Mg}_n\text{H}_{m+2k})]/k \end{aligned} \quad (6)$$

As before, the total energies in the above relations include ZPE corrections.

Looking at the morphology of these clusters in Figure 1 we can make several important observations: As could be expected for small clusters, we can see at a first glance a dramatic reconstruction of the Mg_n skeleton as more and more hydrogens are added. It is also remarkable that the first pair of hydrogen atoms (in the Mg_nH_2 clusters) are located as far as possible away from each other on the “surface” of the cluster, in bridging positions between two or more magnesium atoms. This could be attributed to the optimization of the $\delta+$, $\delta-$ charge distribution.

As more and more hydrogens are added, we can observe the gradual deposition of hydrogen “inside” the cluster. Beyond the “stoichiometric” composition (of $m = 2n$) we can clearly see a pair of hydrogen atoms very close to each other in the form of a H_2 molecule, well outside, but not very far away from the main Mg_nH_{2n} core. This is a clear manifestation of saturation. The additional H_2 molecule is very loosely bound to the Mg_nH_{2n} core, as can be verified from the results in Figure 4b and Figure 5b. In principle, if the resulting oversaturated hydride structure was “sufficiently stable”, it could lead to a much lower sorption energy in the region of $x = 2.1$ – 2.5 , as shown in Figure 4a. However, in this region presumably we have a “molecular adsorption” with a substantially different and much weaker type of binding leading to nonstable structures with a rather “fictitious” low overall desorption energy.

The other region of interest (absorption energies around 40–60 kJ/mol) is the low hydrogen concentration region ($x = 0.25$ – 1.0). Although the behavior of all small nanoclusters in

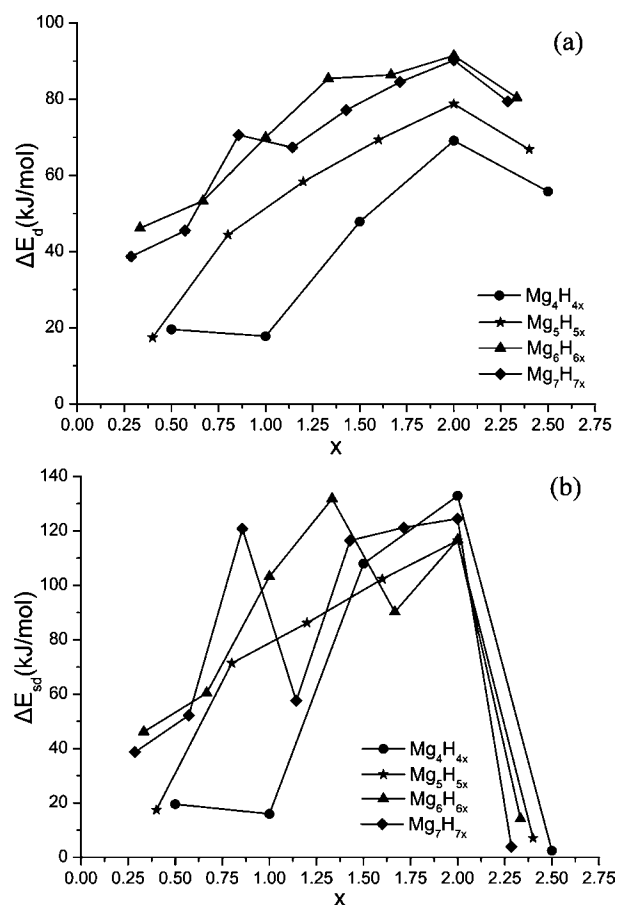


Figure 4. Normalized $[\Delta E_d(\text{Mg}_n\text{H}_m)]$ (a) and stepwise $[\Delta E_{sd}(\text{Mg}_n\text{H}_m)]$ (b) desorption energies, in kJ/mol, for representative Mg_nH_m , $n = 4$ – 7 , $m = 2$ – 16 clusters, obtained at the DFT/M06 level of theory.

Figure 4 is the same near the stoichiometric limit $x \approx 2$, their behavior for $x \ll 2$ is clearly different for different n in the region of $2 \leq n \leq 7$. This is in agreement with the results of Wagemans et al.⁵ For larger (than $n = 6$ – 7) clusters the full dependence of desorption energy on x is more or less similar which allows a more general and “more global” description, which we will attempt to establish on the basis of the results of Figure 5 for the x -dependence of larger Mg_nH_m nanoclusters. As we can see in Figure 5, the results for all Mg_nH_m follow a very similar trend. This allows the introduction of an average fitted (to the results of the $n = 8$ – 19 Mg_nH_m nanoclusters) curve, shown in blue color (dashed line) in the figure, which we will describe further below. In all cases (including the smallest clusters) the stoichiometric composition ($m = 2n$) is the most stable one irrespective of symmetry and geometry (apparently all the way up to the bulk MgH_2) resulting in higher desorption energies at this composition. In this case, $2 \leq x \approx 2$, we have also plotted in Figure 5a some results for the much larger $\text{Mg}_{48}\text{H}_{48x}$ nanocrystal, which have not been included in the fit. Despite the fact that the x -dependence of “crystalline” nanostructures will be further discussed in section 4.2, we should observe here that these results also follow the average behavior of the medium size nanoclusters. For $x > 2$ ($m > 2n$), we have similar (decreasing desorption energy) behavior for all oversaturated structures, including the much larger nanocrystals, with the advantages and disadvantages described earlier for the smaller clusters.

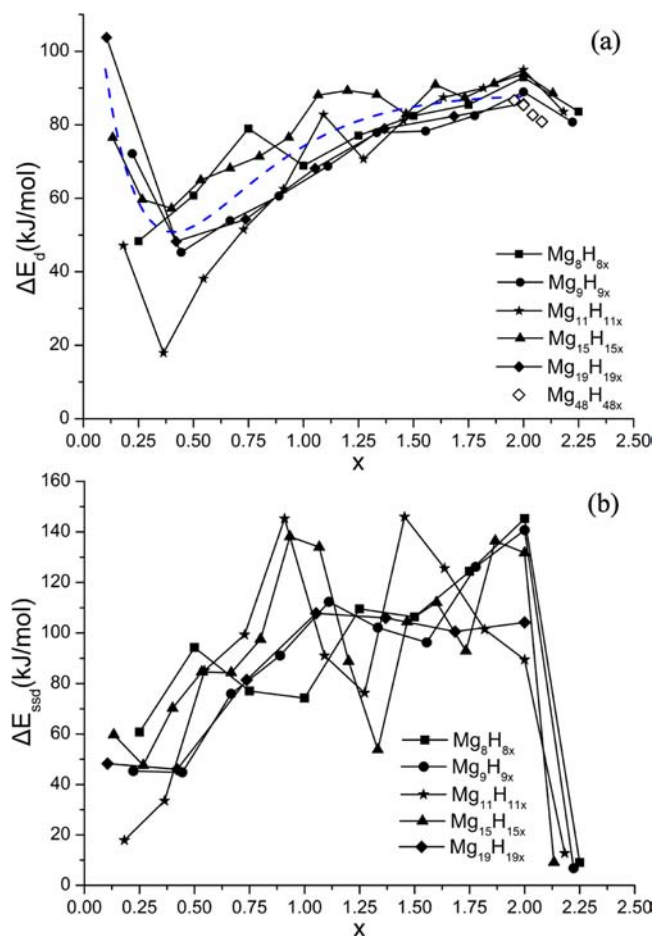


Figure 5. Normalized [$\Delta E_d(Mg_nH_{nx})$] (a) and averaged stepwise [$\Delta E_{ssd}(Mg_nH_{nx})$] (b) desorption energies in kJ/mol, for representative medium and large size Mg_nH_{nx} nanoclusters, obtained at the DFT/M06 level of theory. The continuous (dashed) blue line represents a “fitted average” curve (see text) for $0 < x \leq 2$.

As we can see in Figure 5, the x -dependence in the substoichiometric region ($x \ll 2$) is now more or less uniform, showing a clear dip in the region of $x \cong 0.4$. In this region for which $\Delta E_d(Mg_nH_m)$ would be dominated by the properties of the underlying Mg_n cluster, the increase in $\Delta E_d(Mg_nH_2)$ for very small x (for $m = 2$ in particular) must be a result of a larger and better stabilization of the Mg_nH_2 cluster due to the combined effect of optimization of the Mg–H interaction, through the $\delta+$, $\delta-$ charge distribution optimization (discussed above); together with an improvement of the Mg–Mg interaction. This last contribution to stability is due to the smaller reconstruction of the Mg_n metallic skeleton, for larger n and small m ($m = 2$), which keeps the Mg–Mg interaction in a favorable magnitude. Apparently, due to this last effect, there is no such noticeable abrupt increase in the corresponding ΔE_d curve of Figure 4, for the small clusters. Thus the desorption process in the region of $0.25 \leq x \leq 1$ should be much more efficient, although it could be argued that in this low hydrogen region there would be restrictions compared to the overall hydrogen loading capacity. Nevertheless, in conjunction to a smaller particle size, we could have a significant overall improvement of the storage capacity (and recovery) for a large collection of such substoichiometric nanoclusters distributed in the same volume as a bulk-like nanocrystal. This is in full agreement with the experimental findings of

Schimmel et al.,¹⁰ who report that in a ball-milled nanostructured MgH_2 there may exist a substoichiometric nanostructured MgH_x hydride phase (with $x \ll 2$). Such a hydrogen deficient phase most likely exhibits a much faster diffusion of hydrogen.⁹ Therefore, for “designing” more efficient MgH_x nanostructures for hydrogen storage, it is very important to rationalize this region, or (even better) the full range of x -dependence. To this end, based on the “similarity” of the curves in Figure 5a, we have attempted to construct an average curve, illustrated by a continuous dashed line (in blue color, online) in Figure 5a, describing in a uniform way the expected “average variation with hydrogen content” of the average desorption energy, $\langle \Delta E_d(x) \rangle$, with $x = m/n$. The best possible form we have found, using genetic algorithm fits,³⁸ is

$$\langle \Delta E_d(x; n) \rangle = A - B(2 - x)^a + C(2 - x)^{2a}, \quad (7)$$

$$0 < x \leq 2$$

where $A = 86.0$, $B = -11.5$, $C = 0.9$, and $a = 4$. The constant A in the above relation is in reality weakly dependent on n , and it should be more appropriate to write instead $A = \langle A(n) \rangle$. We have found that $A(n)$ should be of the form

$$A(n) = A_0 + A_1 n^{-1/(3+\delta)}, \quad 0 \leq \delta \leq 0.3 \quad (8)$$

For the time being, the continuous smooth blue curve (dashed line) in Figure 5a should be simply considered as a guide to the eye. These results, especially in conjunction to the size variation of eq 8, have extremely important consequences, as will be further discussed in section 4.

We should also add here that the stepwise desorption curve in Figure 5b gives a clear picture of the relative fraction of the total amount (moles) of hydrogen (and the existing intermediate barriers) which can be desorbed in each step. From this curve, in Figure 5b, it becomes clear that the degree (difficulty) or efficiency of hydrogen absorption is not the same for the whole assumed amount of desorbed hydrogen, for a given $\Delta E_d(Mg_nH_m)$.

4. RESULTS FOR STOICHIOMETRIC $[MgH_2]_N$ NANOCRYSTALS

4.1. Size Dependence. The optimized geometries (at the DFT/M06 level of theory) of the larger stoichiometric $(MgH_2)_N$ nanocrystals ($N = 48, 120, 169$, and 216), based on the bulk MgH_2 structure,⁹ are shown in Figure 6. As we can see in Figure 6, although optimized with low-order symmetry constraints (C_2 or C_5), these nanocrystals are symmetric (of near S_4 symmetry) and “crystalline”. All four nanocrystals have been constructed in a similar “bulk-like” way, and optimized using the same “accurate” method and computational technique. Therefore, the dotted curve which describes the variation of their desorption energy with size (n), in Figure 7, is very smooth and monotonous, in contrast to the same curve for medium and large size “amorphous” nanoclusters as we can see in Figure 7.

This allows a safe (and smooth, as we can see in the figure) extrapolation of $\Delta E_d(MgH_2)_N$ all the way to infinity using the well-known $N^{-1/3}$ dependence.^{13–16} On the basis of this dependence, we have fitted the data of Figure 7 to the continuous line of the form:

$$\Delta E_d(MgH_2)_N = a + bN^{-1/3} \quad (9)$$

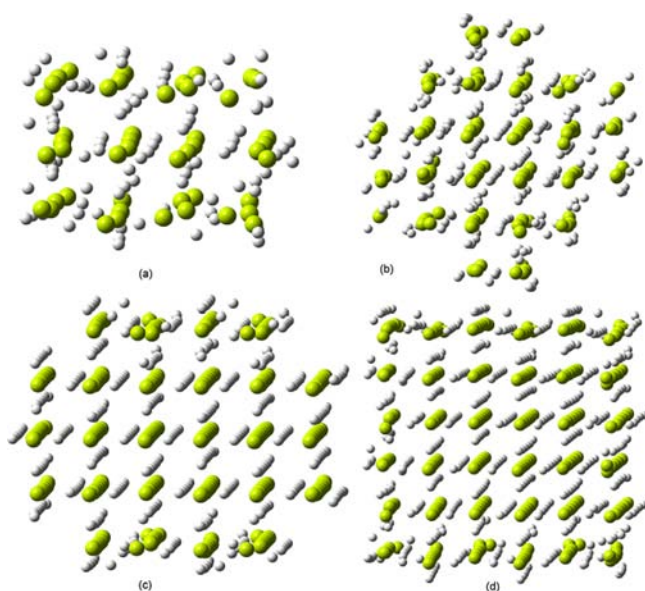


Figure 6. Optimized structures of “crystalline” $(\text{MgH}_2)_N$ nanocrystals for $N = 48$ (a), 120 (b), 169 (c), and 216 (d).

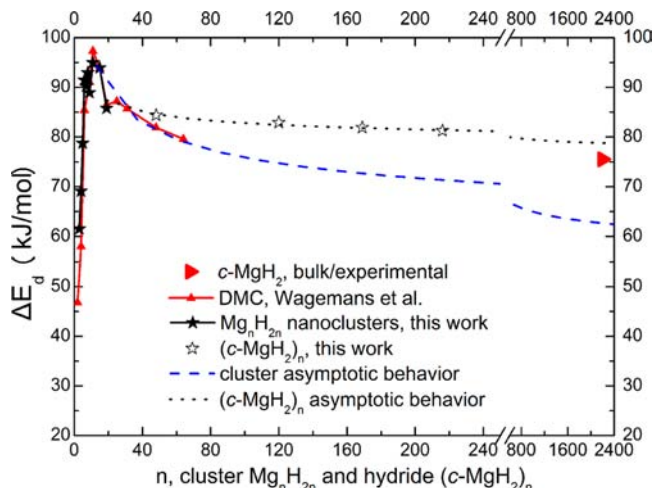


Figure 7. Desorption energy ΔE_d in kJ/mol, of the Mg_nH_{2n} (“non-crystalline”) nanoclusters and the $(\text{MgH}_2)_n$ (“crystalline”) nanocrystals as a function of n , obtained at the DFT/M06 level of theory, together with their extrapolation to infinity.

obtaining $a = 76.5 \pm 1.2$ kJ/mol and $b = 29.0 \pm 5$ kJ/mol. Therefore as $N \rightarrow \infty$, $\Delta E_d(\text{MgH}_2)_N \rightarrow 76.5$ kJ/mol, which is (within chemical accuracy) the measured experimental value of the infinite MgH_2 crystal. We have, thus, obtained with high accuracy the bulk $\Delta E_d(\text{MgH}_2)_N$ value. This type of accuracy was rather unexpected.

In analogy, but not in real similarity, to the bulk-like “crystalline” $(\text{MgH}_2)_n$ nanocrystals, which are structurally and electronically similar, we have attempted to describe the asymptotic variation of ΔE_d for the noncrystalline Mg_nH_{2n} nanoclusters with an “analogous” relation of the form: $\Delta E_d(\text{Mg}_n\text{H}_{2n}) = A_0 + A_1 n^{-(3+\delta)}$, $\delta \geq 0$ of eq 8.

In this form we have allowed for the possible variation of the 3-D exponent 3, to $3+\delta$, through the compensation of a “fractal dimensionality”. Using our results for medium and large nanoclusters we have found $\delta \cong 0.3$ and $A_0 = 54.02$, $A_1 = 86.96$.

The corresponding curve is also shown in the dashed blue curve in Figure 7.

Looking now at this curve in Figure 7, part of which we have seen in Figure 3, we can see that it drops faster than the crystalline curve ($n^{-1/3}$) for large n , approaching asymptotically a lower value ($A_0 = 54.02$) than the crystalline bulk. This value, smaller than 76.5 kJ/mol, but larger than 45 kJ/mol, is in the desirable range for optimal desorption energies (and temperatures), which is very promising for optimal hydrogen storage in MgH_2 nanostructures.

This could be interpreted as a reduction of desorption energy due to some sort of “cellular disorder”. Thus “amorphized” nanostructures would be expected to be much more efficient for hydrogen storage. This interpretation is consistent with experimental evidence that colloidal MgH_2 particles as large as 5 nm are “destabilized”⁷ and the expectation that “amorphous” or “non-crystalline” nanoparticles (larger than 1 nm) could be promising alternatives to crystalline MgH_2 for more efficient hydrogen storage capacities. From the theoretical point of view, the fact that instead of the “crystalline” exponent of 3, we now have a larger $3+\delta$ exponent with a δ value approximately equal to 0.3, corresponds to a surface fractal dimensionality of about 2.2, consistent with experimental estimations (observations).¹²

4.2. Dependence on Hydrogen Content. In analogy to the “non-crystalline” clusters, we have also performed a limited number of hydrogen additions and subtractions in (and from) small “crystalline” nanoclusters such as $\text{Mg}_{48}\text{H}_{96}$, leading to $\text{Mg}_{48}\text{H}_{48x}$ nanocrystals, which were further optimized (without any symmetry constraints). As is indicated in the top of Figure 8, in all cases the additional hydrogens in the form of weakly bound molecules were the most preferred structures with, desorption energies much smaller than the stoichiometric energies, similarly to the noncrystalline clusters, as illustrated earlier in the upper right portion of Figure 5a. It should be emphasized (again) here that the desorption energies of the “crystalline” nanocrystals for the near stoichiometric range $x \cong 2$ fall well within the values predicted (and expected) by the blue fitted curve in Figure 5a for the noncrystalline nanoclusters, not only in the high x region (near $x \cong 2$), but also in the very low x range. Sporadic results in the region of $x \cong 0.45$ for the most favorable $\text{Mg}_{48}\text{H}_{48x}$ nanocrystal seem to verify a very dramatic and drastic reduction of $\langle \Delta E_d(x;n) \rangle$ in this region, as would be expected on the basis of the same curve in Figure 5a, described by eqs 7 and 8. Thus the x -dependence seems to be rather similar (but not identical) for both “crystalline” and “non-crystalline” Mg_nH_{nx} nanostructures. This is very important for “molecular designing” of optimal hydrogen-storing MgH nanocomposite structures, and very encouraging for a near quantitative description of both n and x dependence, which could serve as both extrapolation and/or interpolation formulas. This needs additional work which is currently underway.

5. CONCLUSIONS

We have properly selected and implemented a DFT based, and CCD(T) validated, methodology for the accurate calculation of desorption energy and its variation with size and hydrogen content, in order to locate possible regions of size and hydrogen composition for optimal hydrogen storage in Mg clusters and nanocrystals. Also, we have accurately described and rationalized the size dependence of the desorption energies for Mg_nH_{2n} nanoclusters and $(\text{MgH}_2)_N$ nanocrystals, separately and independently of each other, using general principles and

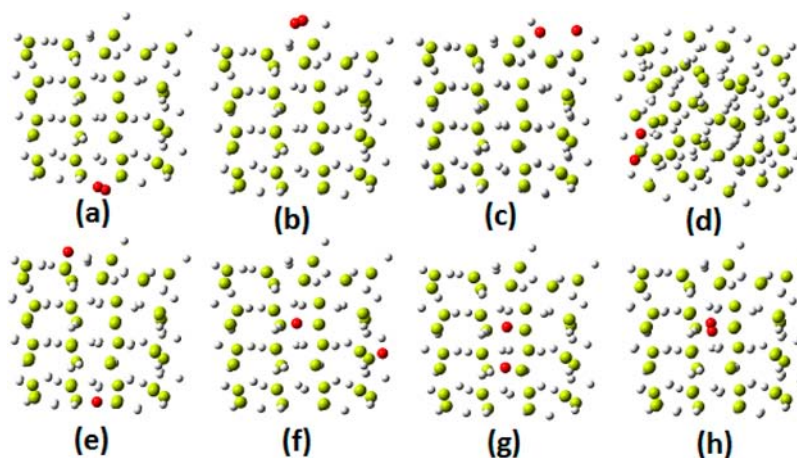


Figure 8. Low-energy structures of $\text{Mg}_{48}\text{H}_{96+2}$ nanocrystals in the order of decreasing stability from top to bottom. Red spheres denote the additional hydrogens.

dimensional arguments. Such a type of analysis allows the development of quantitative relationships which can be used as extrapolation or interpolation formulas for the evaluation/estimation of the desorption energies at various sizes.

We have described and rationalized the absolute and stepwise hydrogen desorption of Mg_nH_m of nonstoichiometric “non-crystalline” nanoclusters. Such analyses have shown that the hydrogen dependence follows a similar pattern for all medium and large size nanoclusters.

The calculated average desorption energy curve for all Mg_nH_{nx} nanoclusters, for $n > 6$, is characterized by a large value at the stoichiometric concentrations $x = 2$, and a strong dip to around 50 kJ/mol for very low substoichiometric concentrations in the region of $x \cong 0.4$. Such behavior is corroborated by the experimental findings.^{9–12} For the near stoichiometry $[\text{MgH}_x]_N$, $x \cong 2$, crystalline nanocrystals, the behavior around the maximum value at $x = 2$ is practically the same. For the stoichiometric $[\text{MgH}_2]_N$ crystalline nanocrystals we have judiciously and very successfully extrapolated the fitted curve, of the form $\Delta E_d(\text{MgH}_2)_N = A + BN^{-1/3}$ to obtain the desorption energy of infinite $(\text{MgH}_2)_N$ bulk hydride with chemical accuracy. For the stoichiometric noncrystalline Mg_nH_{2n} nanoclusters, the fitted curve for the size dependence has a similar but not identical form: $\Delta E_d(\text{Mg}_n\text{H}_{2n}) = A' + B'n^{-1/(3+\delta)}$, with $\delta \cong 0.3$, $A' \cong 54$ kJ/mol.

Contrary to the crystalline nanocrystals, the extrapolated value to infinity (54 kJ/mol) is considerably smaller (and very close to the desired value for applications) than the crystalline bulk value, and the predicted values drop with size much faster. This is highly suggestive that we could have desirable $\Delta E_d(\text{Mg}_n\text{H}_{2n})$ values (around 45–55 kJ/mol) for noncrystalline MgH_2 small-scale particles (powders, colloids, etc.) and nanoparticles of suitable size. This conjecture is in full agreement with experimental evidence that colloidal MgH_2 particles as large as 5 nm are destabilized and that ball-milled MgH_2 samples show considerably lower (45 °C lower) desorption temperatures.

Concerning the stoichiometry and concentration of hydrogen, x , our results clearly show that very low substoichiometric concentrations around $x \cong 0.4$ should be very efficient in substantially reducing desorption energies (and temperatures). This last feature, which is supported by recent experimental observations,^{9,12} in conjunction with reduced particles size and “amorphicity” are, according to our results, the most prominent

directions for most efficient hydrogen storage in magnesium hydride nanocomposite systems.

■ ASSOCIATED CONTENT

📄 Supporting Information

Additional tables as described in the text. This material is available free of charge via the Internet at <http://pubs.acs.org>.

■ AUTHOR INFORMATION

Corresponding Author

koukaras@physics.upatras.gr; zdetsis@upatras.gr

Notes

The authors declare no competing financial interest.

■ REFERENCES

- (1) Kelly, M. T. *Struct. Bonding (Berlin)* **2011**, *141*, 169–201.
- (2) Sakintuna, B.; Lamari-Darkrim, F.; Hirscher, M. *Int. J. Hyd. Storage* **2007**, *32*, 1121–1140.
- (3) Bérubé, V.; Radtke, G.; Dresselhaus, M.; Chen, G. *Int. J. Energy Res.* **2007**, *31*, 637–663.
- (4) Fichtner, M. *Nanotechnology* **2009**, *20*, 204009.
- (5) Wagemans, R. W. P.; van Lenthe, J. H.; de Jongh, P. E.; van Dillen, A. J.; de Jong, K. P. *J. Am. Chem. Soc.* **2005**, *127*, 16675–16680.
- (6) Wu, Z.; Allendorf, M. D.; Grossman, J. C. *J. Am. Chem. Soc.* **2009**, *131*, 13918–13919.
- (7) Aguey-Zinsou, K.-F.; Ares-Fernández, J.-R. *Chem. Mater.* **2008**, *20*, 376–378.
- (8) Varin, R. A.; Czujko, T.; Chiu, C.; Wronski, Z. *J. Alloys Compd.* **2006**, *424*, 356–364.
- (9) Varin, R. A.; Czujko, T.; Wronski, Z. *Nanotechnology* **2006**, *17*, 3856–3865.
- (10) Schimmel, H. G.; Huot, J.; Chapon, L. C.; Tichelaar, F. D.; Mulder, F. M. *J. Am. Chem. Soc.* **2005**, *127*, 14348–14354.
- (11) Fátay, D.; Révész, Á.; Spassov, T. *J. Alloys Compd.* **2005**, *399*, 237–241.
- (12) Deledda, S.; Vennström, M.; Borissova, A.; Yavari, A. R.; Fragneto, G. *Rev. Adv. Mater. Sci.* **2008**, *18*, 616–620.
- (13) Vanithakumari, S. C.; Nanda, K. K. *J. Phys. Chem. B* **2006**, *110*, 1033–1037.
- (14) Qi, W. H.; Wang, M. P.; Zhou, M.; Hu, W. Y. *J. Phys. D: Appl. Phys.* **2005**, *38*, 1429–1436.
- (15) Wautelet, M.; Dauchot, J. P.; Hecq, M. *J. Phys.: Condens. Matter* **2003**, *15*, 3651–3655.
- (16) Farrella, H. H.; Van Siclen, C. D. *J. Vac. Sci. Technol., B* **2007**, *25*, 1441–1447.

- (17) De, S.; Ghasemi, S. A.; Willand, A.; Genovese, L.; Kanhere, D.; Goedecker, S. J. *Chem. Phys.* **2011**, *134*, 124302.
- (18) Lyalin, A.; Solovyov, I. A.; Solovyov, A. V.; Greiner, W. *Phys. Rev. A* **2003**, *67*, 063203.
- (19) Köhn, A.; Weigend, F.; Ahlrichs, R. *Phys. Chem. Chem. Phys.* **2001**, *3*, 711–719.
- (20) Pople, J. A.; Head-Gordon, M.; Raghavachari, K. *J. Chem. Phys.* **1987**, *87*, 5968–5975.
- (21) Raghavachari, K.; Trucks, G. W.; Pople, J. A.; Head-Gordon, M. *Chem. Phys. Lett.* **1989**, *157*, 479–483.
- (22) Prascher, B. P.; Woon, D. E.; Peterson, K. A.; Dunning, T. H.; Wilson, A. K. *Theor. Chem. Acc.* **2011**, *128*, 69–82.
- (23) Frisch, M. J.; Trucks, G. W.; Schlegel, H. B.; Scuseria, G. E.; Robb, M. A.; Cheeseman, J. R.; Scalmani, G.; Barone, V.; Mennucci, B.; Petersson, G. A.; Nakatsuji, H.; Caricato, M.; Li, X.; Hratchian, H. P.; Izmaylov, A. F.; Bloino, J.; Zheng, G.; Sonnenberg, J. L.; Hada, M.; Ehara, M.; Toyota, K.; Fukuda, R.; Hasegawa, J.; Ishida, M.; Nakajima, T.; Honda, Y.; Kitao, O.; Nakai, H.; Vreven, T.; Montgomery, Jr., J. A.; Peralta, J. E.; Ogliaro, F.; Bearpark, M.; Heyd, J. J.; Brothers, E.; Kudin, K. N.; Staroverov, V. N.; Kobayashi, R.; Normand, J.; Raghavachari, K.; Rendell, A.; Burant, J. C.; Iyengar, S. S.; Tomasi, J.; Cossi, M.; Rega, N.; Millam, J. M.; Klene, M.; Knox, J. E.; Cross, J. B.; Bakken, V.; Adamo, C.; Jaramillo, J.; Gomperts, R.; Stratmann, R. E.; Yazyev, O.; Austin, A. J.; Cammi, R.; Pomelli, C.; Ochterski, J. W.; Martin, R. L.; Morokuma, K.; Zakrzewski, V. G.; Voth, G. A.; Salvador, P.; Dannenberg, J. J.; Dapprich, S.; Daniels, A. D.; Farkas, Ö.; Foresman, J. B.; Ortiz, J. V.; Cioslowski, J.; Fox, D. J. *Gaussian 03*, revision C.02; Gaussian, Inc.: Wallingford CT, 2004.
- (24) Perdew, J. P.; Burke, K.; Ernzerhof, M. *Phys. Rev. Lett.* **1996**, *77*, 3865.
- (25) Becke, A. D. *Phys. Rev. A* **1988**, *38*, 3098.
- (26) Perdew, J. P. *Phys. Rev. B* **1986**, *33*, 8822.
- (27) Perdew, J. P.; Burke, K.; Wang, Y. *Phys. Rev. B* **1996**, *54*, 16533.
- (28) Grimme, S. *J. Comput. Chem.* **2006**, *27*, 1787–1799.
- (29) Becke, A. D. *J. Chem. Phys.* **1993**, *98*, 5648–5652.
- (30) Lee, C.; Yang, W.; Parr, R. G. *Phys. Rev. B* **1988**, *37*, 785–789.
- (31) Tao, J. M.; Perdew, J. P.; Staroverov, V. N.; Scuseria, G. E. *Phys. Rev. Lett.* **2003**, *91*, 146401.
- (32) Staroverov, V. N.; Scuseria, G. E.; Tao, J.; Perdew, J. P. *J. Chem. Phys.* **2003**, *119*, 12129.
- (33) Zhao, Y.; Schultz, N. E.; Truhlar, D. G. *J. Chem. Phys.* **2005**, *123*, 161103.
- (34) Zhao, Y.; Truhlar, D. G. *Theor. Chem. Acc.* **2008**, *120*, 215–241.
- (35) *TURBOMOLE*, version 5.6; Universität Karlsruhe: Karlsruhe, Germany, 2000.
- (36) Schmidt, M. W.; Baldridge, K. K.; Boatz, J. A.; Elbert, S. T.; Gordon, M. S.; Jensen, J. H.; Koseki, S.; Matsunaga, N.; Nguyen, K. A.; Su, S.; Windus, T. L.; Dupuis, M.; Montgomery, J. A. *J. Comput. Chem.* **1993**, *14*, 1347–1363.
- (37) Eichkorn, K.; Treutler, O.; Öhm, H.; Häser, M.; Ahlrichs, R. *Chem. Phys. Lett.* **1995**, *240*, 283–289.
- (38) Schmidt, M.; Lipson, H. *Science* **2009**, *324*, 81–85.

■ NOTE ADDED AFTER ASAP PUBLICATION

This paper was published ASAP on September 5, 2012, which was before the author corrections had been applied. The revised version was posted on September 11, 2012.